

See discussions, stats, and author profiles for this publication at: <https://www.researchgate.net/publication/231647332>

# Synthesis, Structure, Electronic, Ionic, and Magnetic Properties of Li<sub>9</sub>V<sub>3</sub>(P<sub>2</sub>O<sub>7</sub>)<sub>3</sub>(PO<sub>4</sub>)<sub>2</sub> Cathode Material for Li-Ion Batteries

ARTICLE in THE JOURNAL OF PHYSICAL CHEMISTRY C · APRIL 2011

Impact Factor: 4.77 · DOI: 10.1021/jp200961b

---

CITATIONS

23

---

READS

44

## 3 AUTHORS, INCLUDING:



Y. M. Zhao

South China University of Technology

100 PUBLICATIONS 1,394 CITATIONS

[SEE PROFILE](#)



Jiantie Xu

Case Western Reserve University

26 PUBLICATIONS 274 CITATIONS

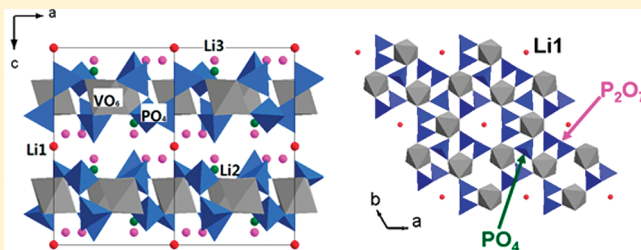
[SEE PROFILE](#)

# Synthesis, Structure, Electronic, Ionic, and Magnetic Properties of $\text{Li}_9\text{V}_3(\text{P}_2\text{O}_7)_3(\text{PO}_4)_2$ Cathode Material for Li-Ion Batteries

Quan Kuang, Yanming Zhao,\* and Jiantie Xu

School of Materials, and School of Physics, South China University of Technology, Guangzhou 510640, People's Republic of China

**ABSTRACT:** Layered monodiphosphate  $\text{Li}_9\text{V}_3(\text{P}_2\text{O}_7)_3(\text{PO}_4)_2$  can be synthesized by direct solid-state reaction using either hydrogen or carbon as the reducing agent at the sintered temperature of 750 °C. When the temperature is higher than 800 °C,  $\text{Li}_9\text{V}_3(\text{P}_2\text{O}_7)_3(\text{PO}_4)_2$  begins to decompose into  $\text{Li}_3\text{V}_2(\text{PO}_4)_3$  and  $\text{Li}_4\text{P}_2\text{O}_7$ . The measurement results of electronic conductivity, magnetization, and electrochemical impedance spectroscopy are reported for the first time. After carbon coating, the electronic conductivity comes to  $2.07 \times 10^{-3} \text{ S cm}^{-1}$ , which is the same order of magnitude as that of carbon-coated  $\text{LiFePO}_4$  and  $\text{Li}_3\text{V}_2(\text{PO}_4)_3$ . Li-ion diffusion coefficient ( $4.19 \times 10^{-10} \text{ cm}^2 \text{ s}^{-1}$ ) for carbon-uncoated  $\text{Li}_9\text{V}_3(\text{P}_2\text{O}_7)_3(\text{PO}_4)_2$  is close to that of  $\text{LiCoO}_2$  and much higher than that of  $\text{LiFePO}_4$ .  $\text{Li}_9\text{V}_3(\text{P}_2\text{O}_7)_3(\text{PO}_4)_2$  exhibits a paramagnetic behavior in the temperature range of 5–300 K, which is consistent with the result from our X-ray photoelectron spectroscopy analysis where the oxidation state of vanadium is +3 in the  $\text{Li}_9\text{V}_3(\text{P}_2\text{O}_7)_3(\text{PO}_4)_2$  compound. The favorable electronic and ionic properties suggest that  $\text{Li}_9\text{V}_3(\text{P}_2\text{O}_7)_3(\text{PO}_4)_2$  can be a potential cathode material for Li-ion batteries.



## 1. INTRODUCTION

Since the commercialization of Li-ion batteries in the 1990s, Li-ion batteries have been widely used in portable equipments and come into service in electric vehicles (EV) and hybrid electric vehicles (HEV) as a sort of storing energy device. Cathode materials have been under intense scrutiny over the past score years to meet the need of high-power and high-capacity applications.<sup>1–5</sup> Safety is one of the most important requirements for commercialized batteries in these areas. The thermal stability of cathode materials during high-current charge and discharge processes is responsible for the safety due to the anhydrous and inflammable electrolyte used in Li-ion batteries. Lithium cobalt oxide  $\text{LiCoO}_2$  as the first generation cathode material for commercialized Li-ion batteries has relatively poor thermal stability and is easy to degrade and tends to lose oxygen during overcharge due to an overlap of the  $\text{Co}^{3+/4+}:\text{t}_{2g}$  band with the top of the  $\text{O}:2p$  band.<sup>6</sup> Since  $\text{LiFePO}_4$  was introduced to the cathode family by Padhi et al. in 1997,<sup>7</sup> this material is already recognized as a promising material and now commercialized as the active cathode for a new generation of Li-ion batteries. All of these achievements are due to its low cost, nontoxic, and remarkable thermal stability attributed to the strong P–O bonds. The restrictions of  $\text{LiFePO}_4$  in high-power application are its low intrinsic electronic conductivity and poor ionic mobility.<sup>8</sup> Ravet et al. have studied the role of the carbon additive and showed that the use of a polymer additive to the precursors can realize the  $\text{Fe}^{3+}$  reduction at low temperature for  $\text{LiFePO}_4$  synthesis and benefit the electronic conductivity from  $\text{sp}^2$ -hybridized carbon deposit.<sup>9</sup>

It is well-known that the layered lithium transitional metal oxides  $\text{LiMO}_2$  ( $\text{M} = \text{Co}, \text{Ni}, \text{Mn}$ ) can offer more efficient ion

transport due to the layered structure given a two-dimension pathway for Li ions.<sup>10–12</sup> Layered isotypic monodiphosphates  $\text{Li}_9\text{M}_3(\text{P}_2\text{O}_7)_3(\text{PO}_4)_2$  ( $\text{M} = \text{Al}, \text{Ga}, \text{Cr}, \text{Fe}$ ), first proposed and synthesized by Poisson et al. via flux method in 1998,<sup>13</sup> are expected to combine high ionic mobility and good thermal stability. Layered monodiphosphate  $\text{Li}_9\text{Ga}_3(\text{P}_2\text{O}_7)_3(\text{PO}_4)_2$  was also obtained by Liu et al. under hydrothermal condition.<sup>14</sup> Recently, Ji and his cooperators investigated the photocatalytic properties of  $\text{Li}_9\text{Fe}_3(\text{P}_2\text{O}_7)_3(\text{PO}_4)_2$  nanoparticles obtained by hydrothermal synthesis.<sup>15</sup> In another aspect, by virtue of the double-electron reaction of vanadium from  $\text{V}^{3+}$  to  $\text{V}^{5+}$ , the Li-rich vanadium phosphates, for example,  $\text{Li}_3\text{V}_2(\text{PO}_4)_3$ <sup>16,17</sup> and  $\text{Li}_5\text{V}(\text{PO}_4)_2\text{F}_2$ ,<sup>18,19</sup> are expected to have high output voltage and good structural stability, and meanwhile export larger discharge specific capacity than that of other transition metal phosphates.

Recently, we have successfully synthesized a new layered monodiphosphate  $\text{Li}_9\text{V}_3(\text{P}_2\text{O}_7)_3(\text{PO}_4)_2$  by the solid-state reaction method.<sup>20</sup> The results show that, in the range of 2.0–4.6 V,  $110 \text{ mAh g}^{-1}$  of discharge capacity is achieved for the carbon-uncoated sample. The Rietveld refinement result of the X-ray diffraction (XRD) data at the end of discharge after the first cycle suggests that the structural reversibility can be retained during electrochemical reactions in  $\text{Li}_9\text{V}_3(\text{P}_2\text{O}_7)_3(\text{PO}_4)_2$ . Via a double-electron reaction of vanadium from  $\text{V}^{3+}$  to  $\text{V}^{5+}$ ,  $\text{Li}_9\text{V}_3(\text{P}_2\text{O}_7)_3(\text{PO}_4)_2$  is expected to deintercalate six Li ions per chemical formula and export a theoretical specific capacity of  $173.45 \text{ mAh g}^{-1}$ .

**Received:** January 28, 2011

**Revised:** March 9, 2011

**Published:** April 04, 2011

Moreover, with a high ratio of phosphorus and vanadium (P:V = 8:3) in the form of monophosphate radicals  $\text{PO}_4$  and diphosphate radicals  $\text{P}_2\text{O}_7$ , monodiphosphate  $\text{Li}_9\text{V}_3(\text{P}_2\text{O}_7)_3(\text{PO}_4)_2$  can be predicted to have favorable thermal stability and high redox potential during charge and discharge due to the inductive effect. These prompt us to investigate the structure and electrochemical properties of  $\text{Li}_9\text{V}_3(\text{P}_2\text{O}_7)_3(\text{PO}_4)_2$  in detail. Here, we have successfully prepared the carbon-coated  $\text{Li}_9\text{V}_3(\text{P}_2\text{O}_7)_3(\text{PO}_4)_2$  using acetylene black in the starting materials. The electronic conductivity, magnetization, and electrochemical impedance spectroscopy (EIS) measurements of  $\text{Li}_9\text{V}_3(\text{P}_2\text{O}_7)_3(\text{PO}_4)_2$  were carried out for the first time. The results demonstrate that this material is a potential candidate for the cathode material in Li-ion batteries.

## 2. EXPERIMENTAL SECTION

The carbon-uncoated  $\text{Li}_9\text{V}_3(\text{P}_2\text{O}_7)_3(\text{PO}_4)_2$  powders were prepared by a conventional solid state reaction using hydrogen as the reducing agent, as shown in our previous work.<sup>20</sup> Likewise, 5 wt % acetylene black was added to the mixture of  $\text{Li}_2\text{CO}_3$ ,  $\text{V}_2\text{O}_5$ , and  $\text{NH}_4\text{H}_2\text{PO}_4$  before the first ball milling to induce formation of carbon-coated  $\text{Li}_9\text{V}_3(\text{P}_2\text{O}_7)_3(\text{PO}_4)_2/\text{C}$  composite sintered in atmosphere of ultrapure Ar via carbon-thermal reaction method. The carbon content was verified by a Vario EL (Elementar, Germany) CHNS Elemental Analyzer, and 7.2% carbon in weight was determined in the final product.

The X-ray diffraction data of  $\text{Li}_9\text{V}_3(\text{P}_2\text{O}_7)_3(\text{PO}_4)_2/\text{C}$  powder for Rietveld refinement analysis were collected by an MXP 18A-HF diffractometer with rotating anode, which had an 18 kW X-ray generator and Cu K $\alpha$  radiation. A graphite monochromator was used for diffracted beams. A step scan mode was adopted with a scanning step of 0.02° and a sampling time of 3 s. The Rietveld refinement of single phase  $\text{Li}_9\text{V}_3(\text{P}_2\text{O}_7)_3(\text{PO}_4)_2$  was carried out by the GSAS program (Larson and Von Dreele, 2000)<sup>21</sup> via the EXPGUI interface (Toby, 2001),<sup>22</sup> and the refinement starting model was chosen on the basis of the  $\text{Li}_9\text{Fe}_3(\text{P}_2\text{O}_7)_3(\text{PO}_4)_2$  compound from the precedent literature.<sup>13</sup> SEM images of  $\text{Li}_9\text{V}_3(\text{P}_2\text{O}_7)_3(\text{PO}_4)_2/\text{C}$  were obtained by using LEO 1530VP (LEO, Germany) scanning electron microscopy (SEM), and energy dispersive spectrometry (EDS) technique was also used to study the chemical composition of the sample sintered at 750 °C. TEM images were carried out with a JEM-2010HR transmission electron microscope (TEM). Electronic conductivity and magnetization measurements were carried out on pellets (~1 mm thick, 10 mm diameter) of  $\text{Li}_9\text{V}_3(\text{P}_2\text{O}_7)_3(\text{PO}_4)_2$  and  $\text{Li}_9\text{V}_3(\text{P}_2\text{O}_7)_3(\text{PO}_4)_2/\text{C}$  powders pressed at 10 MPa and annealed at 600 °C under inert ambient atmosphere. The dc conductivity was measured with the four-probe technique, and the contacts were made with silver paint that are blocking for lithium using the physical property measurement system (PPMS) from QuantumDesign Co. The susceptibility and magnetization were measured with a QuantumDesign SQUID (superconducting quantum interference device) magnetometer, equipped with a 5 T superconducting magnet. The temperature-dependent electronic conductivity and susceptibility data were collected in the temperature ranges of 235–380 and 5–300 K, respectively. The sample temperature was kept constant within ±1 °C during a measurement. The temperature-dependent susceptibility of  $\text{Li}_9\text{V}_3(\text{P}_2\text{O}_7)_3(\text{PO}_4)_2$  was measured in an external magnetic field of 300 G.

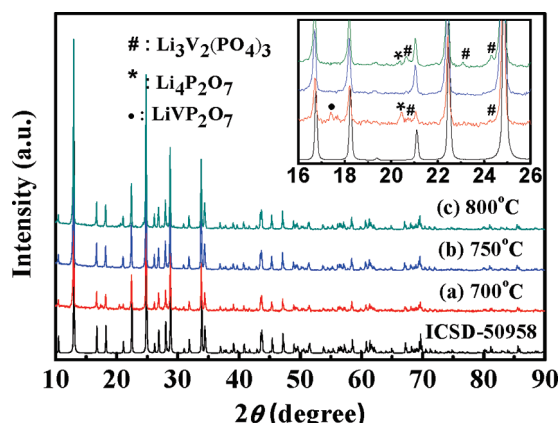


**Figure 1.** X-ray diffraction profiles of  $\text{Li}_9\text{V}_3(\text{P}_2\text{O}_7)_3(\text{PO}_4)_2/\text{C}$  sintered at different temperatures: (a) 700 °C, (b) 750 °C, and (c) 800 °C; (bottom) the data for  $\text{Li}_9\text{Fe}_3(\text{P}_2\text{O}_7)_3(\text{PO}_4)_2$  from ICSD-50958.

The  $\text{Li}_9\text{V}_3(\text{P}_2\text{O}_7)_3(\text{PO}_4)_2$  cathodes of the two-electrode electrochemical cells were fabricated by blending the prepared powder with acetylene black and polyvinylidene fluoride (PVDF) binder at a weight ratio of 80:10:10 in N-methyl-2-pyrrolidone (NMP). The obtained slurry was coated on Al foil, dried at 90 °C for 24 h, and pressed at a pressure of 5 MPa. The fabricated electrodes were dried again at 90 °C for 24 h in vacuum and cut into squares 0.8 cm × 0.8 cm in size. The two-electrode electrochemical cells were assembled in a Mikrouna glovebox filled with high-purity argon, in which lithium metal foil was used as the anode, Celgard 2320 was the separator, and 1 M  $\text{LiPF}_6$  in EC:DMC (1:1, vol %) was the electrolyte. The electrochemical impedance spectroscopy (EIS) of  $\text{Li}_9\text{V}_3(\text{P}_2\text{O}_7)_3(\text{PO}_4)_2$  was performed using a PGSTAT-30 electrochemical station (Autolab). Before EIS measurements, the potential of the positive electrode was set to the requested value and held for 30 min. The concentration of lithium ions in the  $\text{Li}_9\text{V}_3(\text{P}_2\text{O}_7)_3(\text{PO}_4)_2$  lattices then was considered to have reached the equilibrium state. EIS measurements were carried out at four different potentials (3.40, 3.77, 4.10, and 4.52 V), the AC perturbation was 10 mV, and the frequency range was from  $10^5$  Hz to 10 mHz.

## 3. RESULTS AND DISCUSSION

**3.1. Synthesis and Crystal Structure.** The XRD patterns of the  $\text{Li}_9\text{V}_3(\text{P}_2\text{O}_7)_3(\text{PO}_4)_2/\text{C}$  composites sintered at several temperatures via carbon-thermal reaction method show that, at the temperature of 700 °C (Figure 1a), the principal phase is  $\text{Li}_9\text{V}_3(\text{P}_2\text{O}_7)_3(\text{PO}_4)_2$  with  $\text{Li}_3\text{V}_2(\text{PO}_4)_3$ ,  $\text{Li}_4\text{P}_2\text{O}_7$ , and  $\text{LiVP}_2\text{O}_7$  left in the resultants. Single phase  $\text{Li}_9\text{V}_3(\text{P}_2\text{O}_7)_3(\text{PO}_4)_2$  can be formed directly when the temperature reached 750 °C (Figure 1b). This result suggests that the formation of  $\text{Li}_3\text{V}_2(\text{PO}_4)_3$ ,  $\text{Li}_4\text{P}_2\text{O}_7$ , and  $\text{LiVP}_2\text{O}_7$  from the stoichiometric amounts of  $\text{Li}_2\text{CO}_3$ ,  $\text{V}_2\text{O}_5$ , and  $\text{NH}_4\text{H}_2\text{PO}_4$  occurs first at lower sintering temperature, and then the pure  $\text{Li}_9\text{V}_3(\text{P}_2\text{O}_7)_3(\text{PO}_4)_2$  can be obtained through these three intermediate products according to the following reaction when temperatures come to 750 °C:



When the temperature was higher than 800 °C,  $\text{Li}_9\text{V}_3(\text{P}_2\text{O}_7)_3(\text{PO}_4)_2$  began to decompose, and the impurity phases  $\text{Li}_3\text{V}_2(\text{PO}_4)_3$  and  $\text{Li}_4\text{P}_2\text{O}_7$  can be detected (Figure 1c). It suggests that

the structure of  $\text{Li}_3\text{V}_2(\text{PO}_4)_3$  with S.G. (*space group*)  $P2_1/n$  is more stable than that of  $\text{Li}_9\text{V}_3(\text{P}_2\text{O}_7)_3(\text{PO}_4)_2$  with S.G.  $P3c1$  in high temperatures. There are no additional peaks in the XRD pattern of  $\text{Li}_9\text{V}_3(\text{P}_2\text{O}_7)_3(\text{PO}_4)_2/\text{C}$  composite when compared to that of the pristine one.<sup>20</sup> This suggests that the carbon exists as amorphous form, and it agrees well with our TEM results to be mentioned below. It is obvious that the preparation method used here is more suitable for industrialization than are the flux method<sup>13</sup> and hydrothermal approach<sup>14,15</sup> in the future.

To compare the structural difference between carbon-coated and -uncoated compounds, the Rietveld refinement with trigonal space group  $P3c1$  was adopted for  $\text{Li}_9\text{V}_3(\text{P}_2\text{O}_7)_3(\text{PO}_4)_2/\text{C}$ , and the lattice parameters  $a = 9.728(1)$  Å,  $c = 13.591(2)$  Å can be obtained. The reasonably small  $R_p$  (6.8%) and  $R_{wp}$  (10.3%) factors of the Rietveld refinement reveal that single phase carbon-coated  $\text{Li}_9\text{V}_3(\text{P}_2\text{O}_7)_3(\text{PO}_4)_2/\text{C}$  can be obtained under the sintering

**Table 1.** Atomic Sites and Coordinates of  $\text{Li}_9\text{V}_3(\text{P}_2\text{O}_7)_3(\text{PO}_4)_2/\text{C}$  Determined from Rietveld Refinement of High-Power X-ray Diffraction at 300 K

atoms	Wyckoff sites	x	y	z	occupancy
P(1)	4d	2/3	1/3	0.6264(2)	1.00
P(2)	12g	0.3163(2)	0.08942(2)	0.8450(1)	1.00
V	6f	0.5668(2)	0	3/4	1.00
Li(1)	2b	0	0	0	1.00
Li(2)	4d	2/3	1/3	0.8840(18)	1.00
Li(3)	12g	0.3362(9)	0.1036(9)	0.0644(6)	1.00
O(1)	4d	2/3	1/3	0.5156(5)	1.00
O(2)	6f	0.2120(4)	0	3/4	1.00
O(3)	12g	0.6743(3)	0.1863(3)	0.6635(3)	1.00
O(4)	12g	0.4796(3)	0.1054(3)	0.8365(2)	1.00
O(5)	12g	0.3291(3)	0.2537(3)	0.8440(2)	1.00
O(6)	12g	0.2228(3)	-0.0045(4)	0.9353(2)	1.00

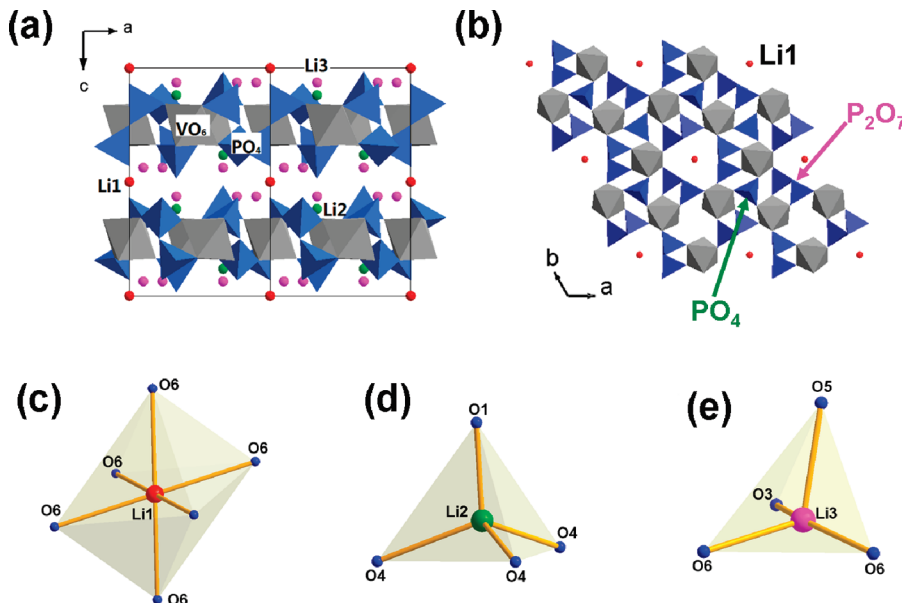


**Figure 2.** The crystal structure diagram of  $\text{Li}_9\text{V}_3(\text{P}_2\text{O}_7)_3(\text{PO}_4)_2$  projected along the  $b$  axis (a), an anionic layer  $\sim[(\text{VP}_2\text{O}_7)_3(\text{PO}_4)_2]^{9-}$  with  $\text{Li}^+$  in the tunnels projected along the  $c$  axis (b), and the coordination environment of  $\text{Li}^+$  (c),  $\text{Li}^+$  (d), and  $\text{Li}^+$  (e). The structures are drawn according to the structural parameters obtained from our Rietveld refinement results. The red, green, and purple spheres indicate  $\text{Li}^+$  ions in three nonequivalent Wyckoff positions  $\text{Li}^+(2b)$ ,  $\text{Li}^+(4d)$ , and  $\text{Li}^+(12g)$ , respectively. The gray octahedra demonstrate the  $\text{VO}_6$  groups, while the blue tetrahedra represent the  $\text{PO}_4$  units. The  $\text{P}_2\text{O}_7$  and  $\text{PO}_4$  anionic units are indicated by purple and green arrows, respectively.

temperature of 750 °C, and no impurity phases can be detected under the resolution of our X-ray diffractometer. The atomic sites and coordinates of  $\text{Li}_9\text{V}_3(\text{P}_2\text{O}_7)_3(\text{PO}_4)_2/\text{C}$  determined from Rietveld refinement are given in Table 1. As we can see in Table 1, the nine lithium atoms per molecular formula occupy three nonequivalent Wyckoff positions  $\text{Li}^+(2b)$ ,  $\text{Li}^+(4d)$ , and  $\text{Li}^+(12g)$ . Three vanadium atoms occupy only one Wyckoff position  $\text{V}^{(6f)}$ . Eight phosphorus atoms occupy two different Wyckoff positions  $\text{P}^{(4d)}$  and  $\text{P}^{(12g)}$ . Twenty-nine oxygen atoms occupy six diverse Wyckoff positions  $\text{O}^{(4d)}$ ,  $\text{O}^{(6f)}$ ,  $\text{O}^{(12g)}$ ,  $\text{O}^{(12g)}$ ,  $\text{O}^{(5)}$ , and  $\text{O}^{(12g)}$ .

$\text{Li}_9\text{V}_3(\text{P}_2\text{O}_7)_3(\text{PO}_4)_2/\text{C}$  is isostructural with those of its Al, Ga, Cr, and Fe analogues.<sup>13–15</sup> It has a two-dimensional layer structure (Figure 2a). The infinite anionic corrugated layers, which are parallel to (001) and separated by  $\text{Li}^+$  cations, consist of  $\text{VO}_6$  octahedra that share corners with  $\text{PO}_4$  tetrahedra and  $\text{P}_2\text{O}_7$  groups (Figure 2b). From the crystal structure diagram of  $\text{Li}_9\text{V}_3(\text{P}_2\text{O}_7)_3(\text{PO}_4)_2/\text{C}$  shown in Figure 2a,b, we can conclude that three nonequivalent lithium ions  $\text{Li}^+(2b)$ ,  $\text{Li}^+(4d)$ , and  $\text{Li}^+(12g)$  may migrate along the 2D pathways parallel to the  $ab$  plane, and  $\text{Li}^+(2b)$  ions may also diffuse along the 1D tunnels paralleled to the  $c$ -axis, which is different from  $\text{LiCoO}_2$  and  $\text{LiFePO}_4$ . Figure 2c–e shows the nearest coordination environment of  $\text{Li}^+(2b)$ ,  $\text{Li}^+(4d)$ , and  $\text{Li}^+(12g)$ , respectively. In the  $\text{Li}^+\text{O}_6$  distorted octahedron,  $\text{Li}^+$  is coordinated by six  $\text{O}^6$  atoms (Figure 2c);  $\text{Li}^+(4d)$  is coordinated by one  $\text{O}^1$  and three  $\text{O}^4$ , and the  $\text{Li}^+\text{O}_4$  tetrahedron exhibits a 3-fold internal symmetry (Figure 2d); and  $\text{Li}^+(12g)$  is coordinated by one  $\text{O}^3$ , one  $\text{O}^5$ , and two  $\text{O}^6$ , which form a distorted tetrahedron (Figure 2e). Both interatomic  $\text{Li}^+$  distance and bottleneck sizes are important factors to consider for understanding ionic conductivity within metal phosphates.<sup>23</sup> Because the diffusion pathways for the  $\text{Li}^+(2b)$ ,  $\text{Li}^+(4d)$ , and  $\text{Li}^+(12g)$  sites in the  $\text{Li}_9\text{V}_3(\text{P}_2\text{O}_7)_3(\text{PO}_4)_2$  structure are still unknown, we only consider the  $\text{Li}^+-\text{O}$  bottleneck within the nearest coordinations. As shown in Table 2,  $\text{Li}^+(2b)$  has the

largest Li–O bottleneck of 2.359 Å, which implies the Li1 ion will be the first one extracted from the matrix along the *c*-axis. After that, Li3 ion with medium Li–O bottleneck of 1.922 Å will be exacted and will hop to the nearest Li site of Li1(2b) or diffuse along the *ab* plane. Li2 ion, which has the smallest Li–O bottleneck of 1.789 Å, is difficult to extract, unless the adequate potential is applied to the cell, and Li2 will hop to the Li3(12g) site. However, there are one Li1, two Li2, and six Li3 per  $\text{Li}_9\text{V}_3(\text{P}_2\text{O}_7)_3(\text{PO}_4)_2$  formula, and the extractions of one Li1 together with five Li3 are sufficient for all  $\text{V}^{3+}$  oxidized to  $\text{V}^{5+}$ . The further extraction of residual Li ions may lead to the collapse of the layer structure.

**3.2. Morphology of Carbon-Coated Composite.** In the previous studies, it has been reported that the morphology and surface area of obtained particles have notable influence on the electrochemical performance of cathode material for Li-ion batteries.<sup>24</sup> Here, the SEM and TEM images were used to identify the morphology of  $\text{Li}_9\text{V}_3(\text{P}_2\text{O}_7)_3(\text{PO}_4)_2/\text{C}$  composite obtained in our experiments, as shown in Figure 3a–d. A particles size of  $\sim 0.5 \mu\text{m}$  with flake-like shape (Figure 3a,c) is smaller than that of the pristine  $\text{Li}_9\text{V}_3(\text{P}_2\text{O}_7)_3(\text{PO}_4)_2$  obtained in the same condition.<sup>20</sup> In addition to the particles size, the nanocarbon particles spread over the surfaces and interspaces of the  $\text{Li}_9\text{V}_3(\text{P}_2\text{O}_7)_3(\text{PO}_4)_2$  grain, which is different from the smooth surface of the bare one.<sup>20</sup> Figure 3b is a representative

**Table 2. Summary of the Size of the Li–O Bottleneck within the Nearest Coordinations and the Distances between the Nearest Li-Sites**

Li–O bottleneck (Å)	nearest Li-site	distance from the nearest Li-site (Å)	
Li1(2b)	2.359	Li3(12g)	3.029
Li2(4d)	1.789	Li3(12g)	3.762
Li3(12g)	1.922	Li1(2b)	3.029

EDS spectrum recorded from the surface analysis of  $\text{Li}_9\text{V}_3(\text{P}_2\text{O}_7)_3(\text{PO}_4)_2/\text{C}$  composite. As expected, the elements of V, P, O, and C can be recorded in the samples, and the result shows that the molar ratio of 2.9:8.0:29.8 for V, P, and O (V:P:O) is close to the theoretical value (3:8:29) based on chemical formula of  $\text{Li}_9\text{V}_3(\text{P}_2\text{O}_7)_3(\text{PO}_4)_2$ . It is difficult to get the information of Li component because of the small atomic number of light elements. In the TEM image in Figure 3c, the amorphous carbon, which connects the adjacent  $\text{Li}_9\text{V}_3(\text{P}_2\text{O}_7)_3(\text{PO}_4)_2$  particles as conductive nanonetwork, can be seen. To show more clearly the carbon-coating characteristic, high-resolution transmission electron microscopy (HRTEM) images are provided. Figure 3d shows the typical lattice-resolved HRTEM image of the  $\text{Li}_9\text{V}_3(\text{P}_2\text{O}_7)_3(\text{PO}_4)_2/\text{C}$  particle shown in Figure 3c. It reveals that the  $\text{Li}_9\text{V}_3(\text{P}_2\text{O}_7)_3(\text{PO}_4)_2/\text{C}$  compound is single crystalline in nature. The lattice spacing of 0.420 nm (Figure 3d) corresponds to the *d*-spacing of the (200) crystal faces, which agrees well with the results indexed on trigonal lattice from the X-ray diffraction patterns of  $\text{Li}_9\text{V}_3(\text{P}_2\text{O}_7)_3(\text{PO}_4)_2/\text{C}$  compounds. As shown in Figure 3d, a layer of carbon is coated on  $\text{Li}_9\text{V}_3(\text{P}_2\text{O}_7)_3(\text{PO}_4)_2/\text{C}$  particles uniformly with a thickness of 8 nm. It is believed that this morphology can enhance the electronic conductivity of the  $\text{Li}_9\text{V}_3(\text{P}_2\text{O}_7)_3(\text{PO}_4)_2/\text{C}$  effectively and improve the electrochemical performance.

**3.3. Electronic Conductivity.** Superior batteries need low internal resistance to reduce voltage polarization and heat release. Therefore, cathode materials for Li-ion batteries should have good conductivities to accomplish the transfer of electrons among the cathode powders and arouse the electrochemical activity. Many efforts have been made on the electronic conductivity of cathode materials for increasing diffusion and ultimately the performance of Li-ion batteries.<sup>25</sup> In an effort to gain a better understanding of the conduction characters in  $\text{Li}_9\text{V}_3(\text{P}_2\text{O}_7)_3(\text{PO}_4)_2$ , a comprehensive study of electronic and ionic conduction phenomena is conducted. The current–voltage test result

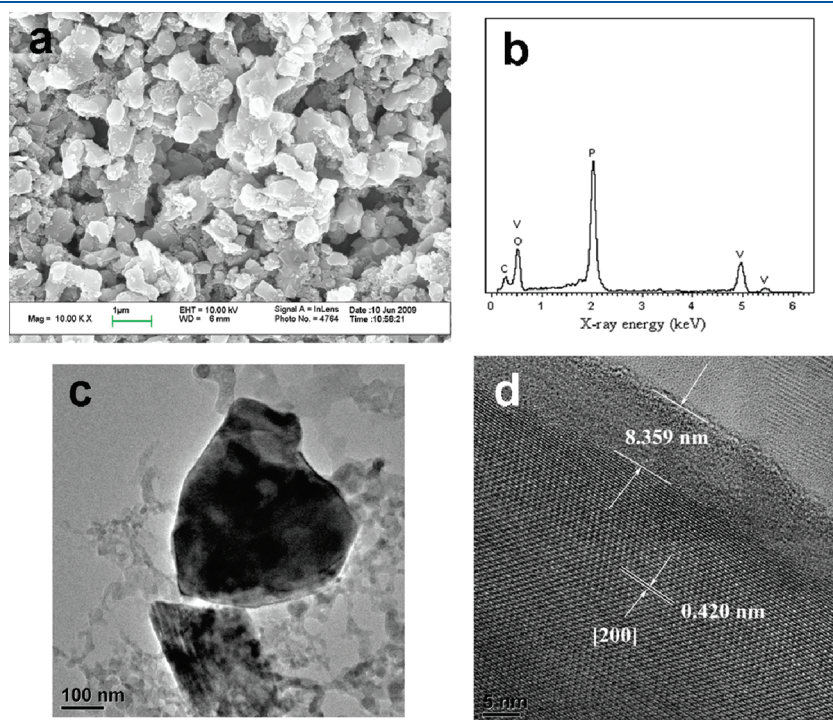


**Figure 3.** (a) SEM, (b) EDS, (c) TEM, and (d) high-resolution TEM images of  $\text{Li}_9\text{V}_3(\text{P}_2\text{O}_7)_3(\text{PO}_4)_2/\text{C}$  composite.

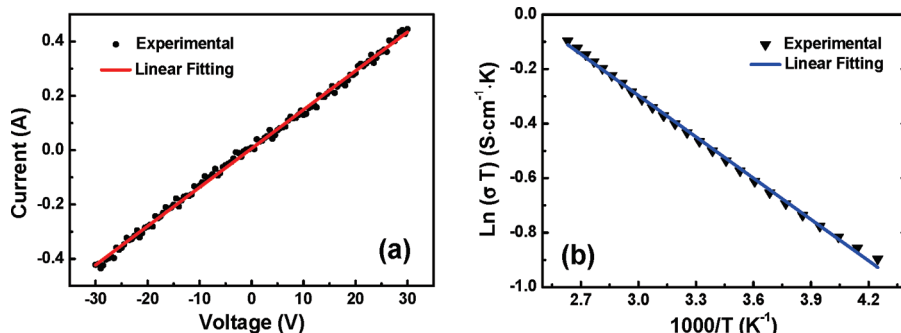


Figure 4. (a) Current–voltage characteristics of  $\text{Li}_9\text{V}_3(\text{P}_2\text{O}_7)_3(\text{PO}_4)_2$  and (b) Arrhenius plots of the electronic conductivity of  $\text{Li}_9\text{V}_3(\text{P}_2\text{O}_7)_3(\text{PO}_4)_2/\text{C}$ .

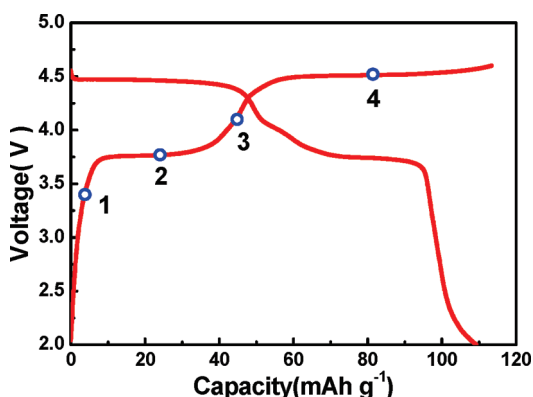


Figure 5. Charge and discharge curves of  $\text{Li}_9\text{V}_3(\text{P}_2\text{O}_7)_3(\text{PO}_4)_2$  from ref 20.

shows ohmic behavior characteristic of pristine  $\text{Li}_9\text{V}_3(\text{P}_2\text{O}_7)_3(\text{PO}_4)_2$  powders (Figure 4a), and no electric capacity or inductance effect can be found under our experimental condition. The linear fitting result in Figure 4a shows that the intrinsic electronic conductivity of  $\text{Li}_9\text{V}_3(\text{P}_2\text{O}_7)_3(\text{PO}_4)_2$  is  $1.43 \times 10^{-8} \text{ S cm}^{-1}$  at room temperature, which is higher than that of  $\text{LiFePO}_4$  ( $\sim 10^{-9} \text{ S cm}^{-1}$ )<sup>26</sup> and has the same order of magnitude as that of  $\text{Li}_3\text{V}_2(\text{PO}_3)_4$  ( $\sim 10^{-8} \text{ S cm}^{-1}$ ).<sup>27</sup> It is expected that the cathode materials are stable and their conductivities maintain nearly unchanged in the temperature range of  $-40$  to  $80$  °C. Here, the electronic conductivity of  $\text{Li}_9\text{V}_3(\text{P}_2\text{O}_7)_3(\text{PO}_4)_2/\text{C}$  is measured in the range of  $-38$  to  $107$  °C (Figure 4b). The electronic conductivity is decreasing nearly linearly with the temperatures, and the conductivity is  $2.07 \times 10^{-3} \text{ S cm}^{-1}$  at room temperature, which is higher than that of the carbon-coated  $\text{Li}_3\text{V}_2(\text{PO}_3)_4$  ( $\sim 10^{-4} \text{ S cm}^{-1}$ ).<sup>28</sup> The electronic conduction is a thermally activated phenomenon and usually follows an Arrhenius-type relationship:<sup>29</sup>

$$\sigma T = \sigma_0 \exp\left(-\frac{E_a}{kT}\right) \quad (1)$$

or

$$\ln(\sigma T) = \ln \sigma_0 - \frac{E_a}{k_B T} \quad (2)$$

where  $\sigma$  is the electronic conductivity,  $\sigma_0$  is the pre-exponential factor,  $E_a$  is the activation energy,  $k_B$  is the Boltzmann constant, and  $T$  is the temperature.

From the slope of the fitting line, the activation energy of  $0.043$  eV was calculated, and it is close to the result of carbon-coated  $\text{LiFePO}_4$  ( $0.045$  eV).<sup>30</sup> The bare layered isotropic monodiphosphates  $\text{Li}_9\text{M}_3(\text{P}_2\text{O}_7)_3(\text{PO}_4)_2$  ( $\text{M} = \text{Al}, \text{Ga}, \text{Cr}, \text{Fe}$ ) are demonstrated to have the conduction activation energy of  $\sim 1$  eV.<sup>13</sup> The carbon coating results in an increase in the electronic conductivity by 5 orders in magnitude for  $\text{Li}_9\text{V}_3(\text{P}_2\text{O}_7)_3(\text{PO}_4)_2$ , which is associated with a decrease in the activation energy to  $0.045$  eV. These results show that the carbon coating is efficient and favorable for practical use. Furthermore, our results show that the electronic conductivity of  $\text{Li}_9\text{V}_3(\text{P}_2\text{O}_7)_3(\text{PO}_4)_2/\text{C}$  has varied by less than 1 order of magnitude in the temperature range of  $-38$  to  $107$  °C, and it suggests that  $\text{Li}_9\text{V}_3(\text{P}_2\text{O}_7)_3(\text{PO}_4)_2$  can be used as the cathode material in wide temperature range conditions in the future.

**3.4. Ionic Diffusion.** As shown in our previous results for the carbon-uncoated  $\text{Li}_9\text{V}_3(\text{P}_2\text{O}_7)_3(\text{PO}_4)_2$ ,<sup>20</sup> two plateaus at  $3.77$  and  $4.52$  V, corresponding to two oxidation peaks in differential capacity profile, can be observed during charge to  $4.6$  V (Figure 5). In the discharge process, two reduction peaks at  $4.39$  and  $3.74$  V are found as well, with low voltage polarization as compared to charge process (Figure 5).<sup>20</sup> To determine the diffusion character of Li ions in different charge states, the electrochemical impedance spectroscopy (EIS) measurements were carried out at four typical voltages of (1)  $3.40$  V, (2)  $3.77$  V, (3)  $4.10$  V, and (4)  $4.52$  V in the charging process of the first cycle illustrated in Figure 5.

Figure 6 shows a sequence of Nyquist plots obtained under various open-circuit condition mentioned above. As the solid electrolyte interface (SEI) has not been formed in the first-charge cycle, only one semicircle and one straight line can be seen in each Nyquist plot. The semicircle with a high frequency intercept on the  $Z'$  (Figure 6a, inset) reveals the cell resistance (of the electrolyte and electrode) of about  $10 \Omega$ , while the semicircle itself elucidates the characteristic of the charge transfer between the electrolyte and the active material  $\text{Li}_9\text{V}_3(\text{P}_2\text{O}_7)_3(\text{PO}_4)_2$ . A very low frequency region of the straight line observed is attributed to the diffusion of the Li ions into the particles of  $\text{Li}_9\text{V}_3(\text{P}_2\text{O}_7)_3(\text{PO}_4)_2$  or the so-called Warburg diffusion. Here, the diffusion coefficients of Li ions can be obtained from the analysis of Warburg impedance.<sup>31</sup> For the  $\text{Li}_9\text{V}_3(\text{P}_2\text{O}_7)_3(\text{PO}_4)_2$  cathode material, the  $\text{Li}^+$  diffusion coefficients  $D_{\text{Li}^+}$  can be estimated from the equation:<sup>32</sup>

$$D_{\text{Li}^+} = \frac{1}{2} \left[ \left( \frac{V_m}{FS\sigma} \right) \left( -\frac{dE}{dx} \right) \right]^2 \quad (3)$$

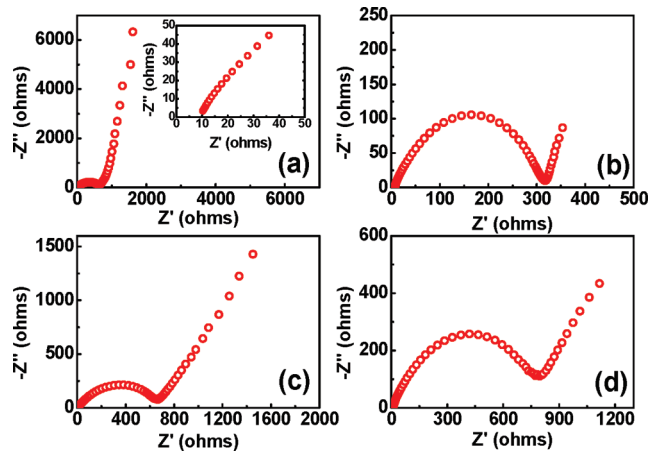


Figure 6. Nyquist plots of  $\text{Li}_9\text{V}_3(\text{P}_2\text{O}_7)_3(\text{PO}_4)_2$  at (a) 3.40 V, (b) 3.77 V, (c) 4.10 V, and (d) 4.52 V in the charging process obtained by EIS measurements.

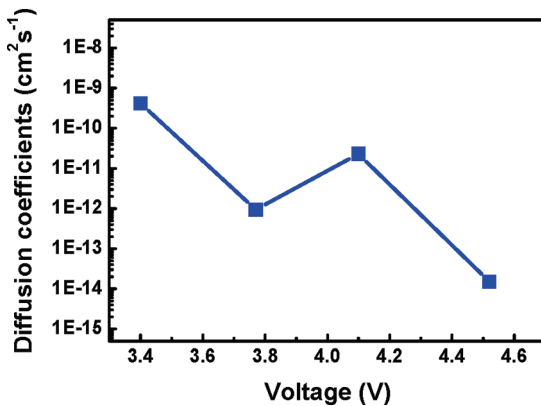


Figure 7. Chemical diffusion coefficients of  $\text{Li}^+$  calculated from the EIS data as a function of cell voltage for  $\text{Li}_9\text{V}_3(\text{P}_2\text{O}_7)_3(\text{PO}_4)_2$  cathode.

where  $V_m$  is the molar volume of  $\text{Li}_9\text{V}_3(\text{P}_2\text{O}_7)_3(\text{PO}_4)_2$  ( $=576.9 \text{ cm}^3 \text{ mol}^{-1}$ ),  $F$  is Faraday's constant,  $S$  is the real surface area of active particles loading on the aluminum foil, and  $\sigma$  is the Warburg coefficient obtained from the slope of the real resistance ( $Z'$ ) versus the inverse square root of the angular frequency ( $\omega^{-1/2}$ ). The value of  $dE/dx$  is the slope of the open-circuit potential versus Li-ion concentration  $x$ .

As shown in Figure 7, the chemical diffusion coefficient of  $\text{Li}^+$  in  $\text{Li}_9\text{V}_3(\text{P}_2\text{O}_7)_3(\text{PO}_4)_2$  deduced from the EIS data is  $4.19 \times 10^{-10}$ ,  $9.44 \times 10^{-13}$ ,  $2.29 \times 10^{-11}$ , and  $1.51 \times 10^{-14} \text{ cm}^2 \text{ s}^{-1}$  at 3.40, 3.77, 4.10, and 4.52 V, respectively. The diffusion coefficient in the uncharged state ( $4.19 \times 10^{-10} \text{ cm}^2 \text{ s}^{-1}$ ) is much higher than that of  $\text{LiFePO}_4$  ( $\sim 10^{-14} \text{ cm}^2 \text{ s}^{-1}$ ) obtained by Prosini et al.,<sup>33</sup> and close to  $\text{LiCoO}_2$  ( $\sim 10^{-10} \text{ cm}^2 \text{ s}^{-1}$ ) and  $\text{LiMn}_2\text{O}_4$  ( $\sim 10^{-10} \text{ cm}^2 \text{ s}^{-1}$ ) reported by Cao et al.<sup>34</sup> and Lu et al.,<sup>35</sup> respectively. The relative higher Li-ions diffusion coefficients in the uncharged state suggest that, as in the  $\text{LiCoO}_2$ , the more efficient Li-ions pathways exist in the layered  $\text{Li}_9\text{V}_3(\text{P}_2\text{O}_7)_3(\text{PO}_4)_2$ . In fact, in the structure of  $\text{Li}_9\text{V}_3(\text{P}_2\text{O}_7)_3(\text{PO}_4)_2$  (as shown in Figure 2a and b), Li ions can, like in layered oxides  $\text{LiMO}_2$  ( $M = \text{Co}, \text{Ni}, \text{Mn}$ ), migrate not only within the interspaces of the anionic corrugated layers  $[\text{V}_3(\text{P}_2\text{O}_7)_3(\text{PO}_4)_2]^{2-}$ , but also along the direction parallel to the  $c$  axis. It should be noted that,

at 3.77 V,  $\text{Li}_9\text{V}_3(\text{P}_2\text{O}_7)_3(\text{PO}_4)_2$  exhibits a lower Li-ion diffusion coefficient than that at 4.10 V, and the plateau zones in the charging curves<sup>20</sup> are suggested to be the two-phase regions at 3.77 V, and it is believed that the transportation of Li ions is hindered at the phase boundaries. It is a common phenomenon of chemical diffusion coefficient in the cathode materials, which show a phase transition for strong attractive interactions between the intercalation species and the host matrix or some order-disorder transition during cycling.<sup>36</sup>

Possion et al. have shown that the layered isotropic monodiphosphates  $\text{Li}_9\text{M}_3(\text{P}_2\text{O}_7)_3(\text{PO}_4)_2$  exhibit a Li-ion conduction mainly parallel to (001);<sup>13</sup> the diffusions of Li ions are much more facile along the  $c$  axis than those within the interspaces of the anionic corrugated layers. From the coordination environment analysis of three different Li sites with different site energy due to the higher Coulombic interactions with  $\text{PO}_4$  and  $\text{P}_2\text{O}_7$  units as compared to the layered oxides  $\text{LiMO}_2$ , it can also be seen that Li1 is the easiest extraction one among three Li ions (Figure 2a,b). Thus, the first plateau voltage of 3.77 V should be corresponding to the extraction of Li1 along the (001) direction. On the other hand, the second plateau voltage of 4.52 V is corresponding to the extraction of Li3 (with higher site energy), which can only diffuse within the anionic layers. Therefore, it is not difficult to understand why the diffusion coefficient is decreasing when charging to higher voltage even in the single phase region. Moreover, some side reactions of electrolyte may also exist in relatively high voltage. The higher diffusion coefficients observed when the voltages (3.40 and 4.10 V) are far away from the plateau zones (3.77 and 4.52 V) suggest the easier hopping of the Li-ion existing in the single phase structure.<sup>37</sup>

**3.5. Magnetic Properties.** Magnetic properties of lithium intercalation compounds, such as  $\text{LiMO}_2$  ( $M = \text{Ni}, \text{Fe}, \text{Mn}$ ),  $\text{LiMn}_2\text{O}_4$ ,  $\text{LiCoMnO}_4$ , and  $\text{LiMPO}_4$  ( $M = \text{Ni}, \text{Fe}, \text{Mn}$ ), have been extensively investigated.<sup>38</sup> Here, we report for the first time the magnetic characters of layered monodiphosphates  $\text{Li}_9\text{V}_3(\text{P}_2\text{O}_7)_3(\text{PO}_4)_2$ . Figure 8a shows the temperature dependence of the susceptibility ( $\chi(T)$ ) measured in a field of 300 Oe using a superconducting quantum interference device (SQUID) magnetometer. We find a match of  $\chi^{-1}(T)$  from Curie–Weiss law in the temperature range of 150–300 K (inset of Figure 8a), which is evidence of the paramagnetic behavior of  $\text{Li}_9\text{V}_3(\text{P}_2\text{O}_7)_3(\text{PO}_4)_2$ . The field dependence of the magnetizations measured at 5, 50, and 300 K are shown in Figure 8b. The data with no hysteresis and remanent magnetization clearly demonstrate the presence of paramagnetic behavior in the temperature range of 5–300 K. The absence of magnetic ordering might be related to frustration in such a structure. From the linear fit of the susceptibility data restricted to the temperature range of  $T > 150$  K according to the Curie–Weiss law:

$$\chi = \frac{C}{T - \theta} \quad (4)$$

the Curie constant  $C$  ( $=1.05 \text{ emu Oe}^{-1} \text{ mol}^{-1}$ ) and Weiss coefficient  $\theta$  ( $=-21.45 \text{ K}$ ) can be obtained. The value of effective momentum number can be estimated using the following equation:

$$p_{\text{eff}} = \left( \frac{3k_B C}{N_A \mu_B^2} \right)^{1/2} \quad (5)$$

where  $k_B$  is the Boltzmann constant,  $N_A$  is the molar concentration of vanadium ions, and  $\mu_B$  is the Bohr magneton. The magnetic moment per  $\text{V}^{3+}$  ion,  $2.91 \mu_B$ , is calculated for

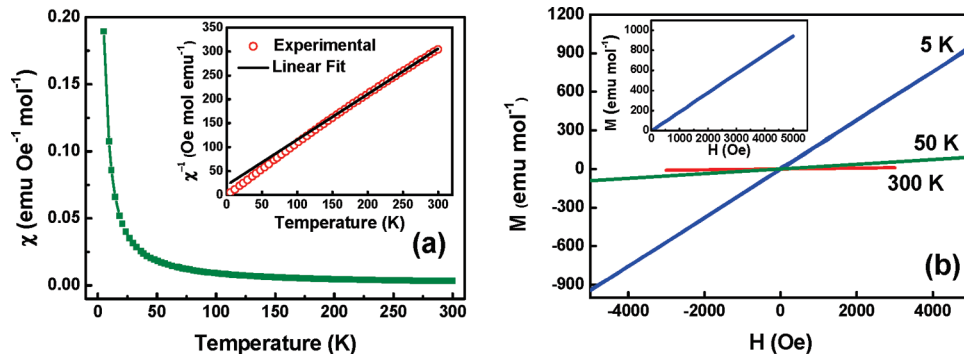


**Figure 8.** (a) The temperature dependence of the molar susceptibility and inverse susceptibility (inset); and (b) the magnetization dependence of the applied field at the temperature of 5, 50, and 300 K, and the magnetization process at 5 K (inset) of  $\text{Li}_9\text{V}_3(\text{P}_2\text{O}_7)_3(\text{PO}_4)_2$ .

$\text{Li}_9\text{V}_3(\text{P}_2\text{O}_7)_3(\text{PO}_4)_2$ , which is slightly larger than the value of the theoretical moment of  $2.83 \mu_B$  for  $\text{V}^{3+}(3d^2)$  ion as well as the  $2.85 \mu_B$  for  $\text{V}^{3+}$  ion in  $\text{VPO}_4 \cdot \text{H}_2\text{O}$ .<sup>39</sup> The slightly larger value of the effective magnetic moment is consistent with the result from our X-ray photoelectron spectroscopy (XPS) analysis where the oxidation state of vanadium is +3 in the  $\text{Li}_9\text{V}_3(\text{P}_2\text{O}_7)_3(\text{PO}_4)_2$  compound<sup>20</sup> and implies there is not a single contribution of  $\text{V}^{3+}$  to the magnetic susceptibility, which might be due to the magnetic polarons associated with Li vacancies, like in  $\text{LiFePO}_4$ . The fit of data below 150 K, especially below 50 K, is hopeless because all of the compounds with transition metals contain residual impurities that contribute a Curie law at low temperature, and this contribution below 50 K becomes non negligible even if the impurity concentration is too small to be detected by XRD, due to the  $T^{-1}$  divergence of the Curie law.

#### 4. CONCLUSIONS

In this Article, the results of electronic conductivity, magnetization, and electrochemical impedance spectroscopy (EIS) measurements for  $\text{Li}_9\text{V}_3(\text{P}_2\text{O}_7)_3(\text{PO}_4)_2$  compound are reported for the first time. Single phase trigonal sample of  $\text{Li}_9\text{V}_3(\text{P}_2\text{O}_7)_3(\text{PO}_4)_2$  can be synthesized by direct solid-state reaction using either hydrogen or carbon as the reducing agent at the sintered temperature of 750 °C. When the temperature is higher than 800 °C,  $\text{Li}_9\text{V}_3(\text{P}_2\text{O}_7)_3(\text{PO}_4)_2$  begins to decompose into  $\text{Li}_3\text{V}_2(\text{PO}_4)_3$  and  $\text{Li}_4\text{P}_2\text{O}_7$ . After carbon coating, the electronic conductivity can increase from  $1.43 \times 10^{-8} \text{ S cm}^{-1}$  for carbon-uncoated to  $2.07 \times 10^{-3} \text{ S cm}^{-1}$ ; the latter is of the same order of magnitude as that of carbon-coated  $\text{LiFePO}_4$  and  $\text{Li}_3\text{V}_2(\text{PO}_3)_4$ . Our results show that Li-ion diffusion coefficient ( $4.19 \times 10^{-10} \text{ cm}^2 \text{ s}^{-1}$ ) for carbon-uncoated  $\text{Li}_9\text{V}_3(\text{P}_2\text{O}_7)_3(\text{PO}_4)_2$  is close to that of  $\text{LiCoO}_2$  and much higher than that of  $\text{LiFePO}_4$ . The magnetic measurement results reveal that  $\text{Li}_9\text{V}_3(\text{P}_2\text{O}_7)_3(\text{PO}_4)_2$  exhibits a paramagnetic behavior in the temperature range of 5–300 K, which is consistent with the result from our X-ray photoelectron spectroscopy analysis where the oxidation state of vanadium is +3 in the  $\text{Li}_9\text{V}_3(\text{P}_2\text{O}_7)_3(\text{PO}_4)_2$  compound. The layered monodiphosphate  $\text{Li}_9\text{V}_3(\text{P}_2\text{O}_7)_3(\text{PO}_4)_2$  with its favorable electronic, ionic, and magnetic properties is promising great potential for future applications as a cathode material in Li-ion batteries.

#### ■ AUTHOR INFORMATION

##### Corresponding Author

\*Tel.: +86 20 87111963. Fax: +86 20 87112837. E-mail: zhaoym@scut.edu.cn.

#### ■ ACKNOWLEDGMENT

This work was funded by an NSFC Grant (no. 50972046) supported through the NSFC Committee of China and the Foundation (no. 07118058) supported through the Science and Technology Bureau of Guangdong Government, respectively. We are indebted to Prof. Cheng Dong from the Institute of Physics, Chinese Academy of Science, and Prof. Dong Shu from the School of Chemistry and Environment, South China Normal University, for their assistance with the X-ray diffraction and electrochemical impedance spectroscopy experiments, respectively.

#### ■ REFERENCES

- Winter, M.; Brodd, R. J. *Chem. Rev.* **2004**, *104*, 4245.
- Whittingham, M. S. *Chem. Rev.* **2004**, *104*, 4271.
- Li, H.; Wang, Z. X.; Chen, L. Q.; Huang, X. *J. Adv. Mater.* **2009**, *21*, 4593.
- Goodenough, J. B.; Kim, Y. *Chem. Mater.* **2010**, *22*, 587.
- Ellis, B. L.; Lee, K. T.; Nazar, L. F. *Chem. Mater.* **2010**, *22*, 691.
- Chebiam, R. V.; Prado, F.; Manthiram, A. *Chem. Mater.* **2001**, *13*, 2951.
- Padhi, A. K.; Nanjundaswamy, K. S.; Goodenough, J. B. *J. Electrochem. Soc.* **1997**, *144*, 1188.
- Zane, D.; Carewska, M.; Scaccia, S.; Cardellini, F.; Prosini, P. P. *Electrochim. Acta* **2004**, *49*, 4259.
- Ravet, N.; Gauthier, M.; Zaghib, K.; Goodenough, J. B.; Mauger, A.; Gendron, F.; Julien, C. M. *Chem. Mater.* **2007**, *19*, 2595.
- Mitzushima, K.; Jones, P. C.; Wiseman, P. J.; Goodenough, J. B. *Mater. Res. Bull.* **1980**, *15*, 783.
- Dahn, J. R.; Sacken, U. V.; Juzkow, M. W.; Al-Janaby, H. *J. Electrochem. Soc.* **1991**, *138*, 2207.
- Armstrong, A. R.; Bruce, P. G. *Nature* **1996**, *381*, 499.
- Poisson, S.; d'Yvoire, F.; Dung, N.-H.; Bretey, E.; Berthet, P. *J. Solid State Chem.* **1998**, *138*, 32.
- Liu, X.-X.; Wang, C. X.; Luo, S. M.; Mi, J. X. *Acta Crystallogr.* **2006**, *E62*, i112.
- Ji, F.; Li, C. L.; Zhang, J. H. *Appl. Mater. Interfaces* **2010**, *2*, 1674.
- Gaubicher, J.; Wurm, C.; Goward, G.; Masquelier, C.; Nazar, L. *Chem. Mater.* **2000**, *12*, 3240.
- Saidi, M. Y.; Barker, J.; Huang, H.; Adamson, G. *Electrochim. Solid-State Lett.* **2002**, *5*, A149.
- Yin, S.-C.; Herle, P. S.; Higgins, A.; Taylor, N. J.; Makimura, Y.; Nazar, L. F. *Chem. Mater.* **2006**, *18*, 1745.
- Makimura, Y.; Cahill, L. S.; Iriyama, Y.; Goward, G. R.; Nazar, L. F. *Chem. Mater.* **2008**, *20*, 4240.
- Kuang, Q.; Xu, J. T.; Zhao, Y. M.; Chen, X. L.; Chen, L. Q. *Electrochim. Acta* **2011**, *56*, 2201.
- Larson, A. C.; Von Dreele, R. B. *Los Alamos National Laboratory Report*, 2004, LAUR 86-748.

- (22) Toby, B. H. *J. Appl. Crystallogr.* **2001**, *34*, 210–213.
- (23) Cahill, L. S.; Chapman, R. P.; Britten, J. F.; Goward, G. R. *J. Phys. Chem. B* **2006**, *110*, 7171.
- (24) Huang, H.; Yin, S.-C.; Kerr, T.; Taylor, N.; Nazar, L. F. *Adv. Mater.* **2002**, *14*, 1525.
- (25) Park, M.; Zhang, X.; Chung, M.; Less, G. B.; Sastry, A. M. *J. Power Sources* **2010**, *195*, 7904.
- (26) Herle, P. S.; Ellis, B.; Coombs, N.; Nazar, L. F. *Nat. Mater.* **2004**, *3*, 147.
- (27) Yin, S.-C.; Strobel, P. S.; Grondyey, H.; Nazar, L. F. *Chem. Mater.* **2004**, *16*, 1456.
- (28) Chen, Y. H.; Zhao, Y. M.; An, X. N.; Liu, J. M.; Dong, Y. Z.; Chen, L. *Electrochim. Acta* **2009**, *54*, 5844.
- (29) Antolini, E. *Solid State Ionics* **2004**, *170*, 159.
- (30) Zaghib, K.; Mauger, A.; Goodenough, J. B.; Gendron, F.; Julien, C. M. *Chem. Mater.* **2007**, *19*, 3740.
- (31) Tang, A. P.; Wang, X. Y.; Xu, G. R.; Zhou, Z. H.; Nie, H. D. *Mater. Lett.* **2009**, *63*, 1439.
- (32) Zhang, D.; Popov, B. N.; White, R. E. *J. Power Sources* **1998**, *76*, 81.
- (33) Prosini, P. P.; Lisi, M.; Zane, D.; Pasquali, M. *Solid State Ionics* **2002**, *148*, 45.
- (34) Cao, Q.; Zhang, H. P.; Wang, G. J.; Xia, Q.; Wu, Y. P.; Wu, H. Q. *Electrochem. Commun.* **2007**, *9*, 1228.
- (35) Lu, D. S.; Li, W. S.; Zuo, X. X.; Yuan, Z. Z.; Huang, Q. M. *J. Phys. Chem. C* **2007**, *111*, 12067.
- (36) Rui, X. H.; Ding, N.; Liu, J.; Li, C.; Chen, C. H. *Electrochim. Acta* **2010**, *55*, 2384.
- (37) Liu, S. Q.; Li, S. C.; Huang, K. L.; Gong, B. L.; Zhang, G. *J. Alloys Compd.* **2008**, *450*, 499.
- (38) Julien, C. M.; Ait-Salah, A.; Mauger, A.; Gendron, F. *Ionics* **2006**, *12*, 21.
- (39) Vaughey, J. T.; Harrison, W. T. A.; Jacobson, A. J.; Goshorn, D. P.; Johnson, J. W. *Inorg. Chem.* **1994**, *33*, 2481.